



Kinetics of Hydrogenation of Acetic Acid to Ethanol

QIANG CHEN^{*ID}, XUEBING ZHANG, SHUXUN TIAN, JUNYING LONG, XIANGKUN MENG, QI SUN^{ID} and YONGLONG LI

National Institute of Clean-and-Low-Carbon Energy, Beijing 102211, P.R. China

*Corresponding author: E-mail: qiang.chen.cx@chnenergy.com.cn

Received: 18 June 2019;

Accepted: 20 August 2019;

Published online: 16 November 2019;

AJC-19641

The intrinsic kinetic behaviour of catalytic hydrogenation of acetic acid in vapour phase was studied over a multi-metallic catalyst. The rate expression was derived from the sequence of elementary reaction steps based on a Langmuir-Hinshelwood-model involving two types of active sites. Experiments were carried out in a fixed bed reactor, which is similar to an isothermal integral reactor designed to excluding the negative effects of internal and external diffusion. The reaction conditions investigated were as follow: reaction temperature 275-325 °C, reaction pressure 1.5-3.0 MPa, liquid hourly space velocity (sv) 0.3-1.2 h⁻¹, molar ratio of hydrogen to acetic acid (H/AC) 8:20. The results show that conversion of acetic acid increases with increasing the reaction temperature and pressure, but decreases with increasing the space velocity and H/AC. Furthermore, reducing the reaction pressure and increasing reaction temperature, space velocity and H/AC can improve the reaction selectivity of acetic acid to ethanol. The established kinetic model results agreed with experimental results. The relative difference between the calculated value and the experimental value is less than 6 %. The values of model parameters are consistent with the three thermodynamic constraints. The study provided evidence that the intrinsic kinetic model is suitable both mathematically and thermodynamically, and it could be useful in guiding reactor design and optimization of operating conditions.

Keywords: Kinetics, Hydrogenation, Esterification, Integral reactor, Conversion, Selectivity, Model.

INTRODUCTION

Ethanol is currently the largest produced alternative energy world-widely to petroleum-derived engine fuels due to its compatibility within existing spark-ignition engines and its relatively well-developed production technologies [1]. Most of the studies have broadly asserted that vehicle efficiency increases with ethanol use to justify reducing the greenhouse gas impact of ethanol [2,3].

Ethanol is produced by hydration of ethylene [4-6] or fermentation of biomass that has sugar, starch or cellulose [3,7]. Hydration of ethylene is a proven industrial process [4], but it relies on availability and cost of ethane. Presently, the production of ethanol by fermentation of carbohydrates is the primary route for gasoline additive in America, Brazil and Europe [8,9]. However, it depends on availability of land area, soil, water, price of feedstocks and even the local policy, which is very limited for most of the countries [3]. Hence, there is a drive to explore new fuel production methods to meet the increasing fuel demand. One method is the conversion of carbon-based feedstocks, such

as biomass, coal, or natural gas, to syngas, which can then be converted catalytically to ethanol and higher alcohols [2,10].

During the past few years, urban air pollution has become a serious problem and attracted great public attention in China. The main source of emissions is vehicle exhaust [11,12]. Fuel ethanol is one of the most promising choices that can reduce emissions [13]. The plan to promote ethanol gasoline for motor vehicles throughout the country by 2020 was published by the government of China in September 2017. Due to the shortage of oil and gas resources, ethanol is mainly produced by fermentation of corns in China. In this process, feedstock cost normally accounts for over 80 % of the total cost. It can be found that corn price has been more than doubled over the past decade. As the subsidy for corn ethanol producers gradually phased out over recent years, the profit of producing corn ethanol became lower or even negative [14]. Coal accounts for over 60 % of China's total primary energy consumption and will inevitably remain the overwhelming indigenous energy resource for the foreseeable future. The method of ethanol production using syngas from coal gasification is suitable for China's

actual condition. For this reason, many Chinese researchers have carried out the study of coal to ethanol technology.

Ethanol can be produced from both syngas directly and other various sources such as acetic acid, ethyl acetate, methyl acetate and dimethyl ether, which are converted from syngas [15]. Research on the production of alcohols from syngas directly has been going on for decades, however the reaction exhibits poor selectivity of ethanol and remains challenging [2]. The processes of syngas to methanol [16,17] and carbonylation of methanol to acetic acid [18] are mature technologies. Thus, the hydrogenation process of acetic acid to ethanol is a promising choice.

Many patents have reported the catalysts for hydrogenation of acetic acid. In these studies, most of the catalysts were one or more noble metals in Group VIII, dispersed on Group III or IV metal oxides. Rachmady and Vannice [19-23] carried out a series of researches on platinum catalysts supported on TiO_2 , SiO_2 , Al_2O_3 and Fe_2O_3 , and the results were compared with that obtained without support. Several observations were made about the kinetic behaviour of acetic acid hydrogenation to form organic compounds over supported platinum catalysts: (a) the reaction requires both metal and an appropriate oxide phase in the catalyst; (b) oxides that are active for ketonization are the best supports, implying the reaction can occur on the oxide surface; (c) platinum acts as a source of activated hydrogen, presumably hydrogen atoms [19]. Based on these findings, a Langmuir-Hinshelwood-type mechanism was proposed, in which acetaldehyde is formed as the first initial product, and it can react with additional hydrogen atoms to form ethanol [19,22]. The reaction model similar to that used to describe acetic acid reduction over Pt/ TiO_2 was applied to this reaction over Fe/ SiO_2 , with the only difference being that the rate-determining steps involved the addition of the first H atom to an acetate species [19] rather than an acyl species [22]. Non-local density functional theory (DFT) calculations were used to examine alternative mechanisms for the hydrogenation of acetic acid to ethanol over different catalysts [24]. Using the overall reaction energies to deduce a plausible mechanism for acetic acid hydrogenolysis, Pallassana and Neurock [24] found that the acetyl formation and acetyl hydrogenation to

acetaldehyde appear to be kinetically significant steps. The investigations showed that Pt/Sn-based catalysts are selective for conversion of acetic acid to form acetaldehyde and ethanol, whereas platinum catalysts completely decompose acetic acid to gas productions [25-27]. Additionally, Zhang [27] added esterification of acetic acid and ethanol to ethyl acetate occurred on the oxide surface to the elementary steps, therefore, selectivity of ethanol was led into the kinetics model. A more recent study of hydrogenation of acetic acid over alumina or silica supported Cu/In and Ni/In catalysts was carried out, and the results showed that the activity dependence on the reactant partial pressures denotes the rate-determining surface reaction in terms of Langmuir-Hinshelwood kinetics [28,29].

Within all reported catalysts, it was difficult to obtain a high conversion of acetic acid while keep a high selectivity of ethanol simultaneously. Our research group developed a multi-metallic based catalyst, which was proven to be more efficiency in both conversion and selectivity. At this point, investigating the kinetics behaviour of hydrogenation reaction of acetic acid to ethanol over this multi-metallic based catalyst becomes critical to scale up in the future.

EXPERIMENTAL

Acetic acid (99.5 % purity) was supplied by Sinopharm Chemical Reagent Co. Ltd., China. Hydrogen from Air Liquide (China) Holding Co. Ltd. was 99.99 vol. %. The kinetic tests were carried out on a multi-metallic catalyst.

Procedure: Hydrogenation of acetic acid system is shown in Fig. 1. High pressure hydrogen from the cylinder was depressurized by a pressure reducing valve, and the hydrogen flow rate was regulated by a mass flow controller. The acetic acid was pumped into the reaction system and was well mixed with hydrogen by an on-line mixer. A fixed bed reactor similar to an isothermal integral reactor was used for the kinetics testing. Acetic acid was heated to vapour phase in the front of reactor. Hydrogenation reaction was down in the catalyst bed located in the mid of reactor. The final products were cooled through a condenser and entered a gas liquid separator tank. The liquid products including ethanol, ethyl acetate, acetaldehyde, other trace components and unreacted acetic acid were collected at

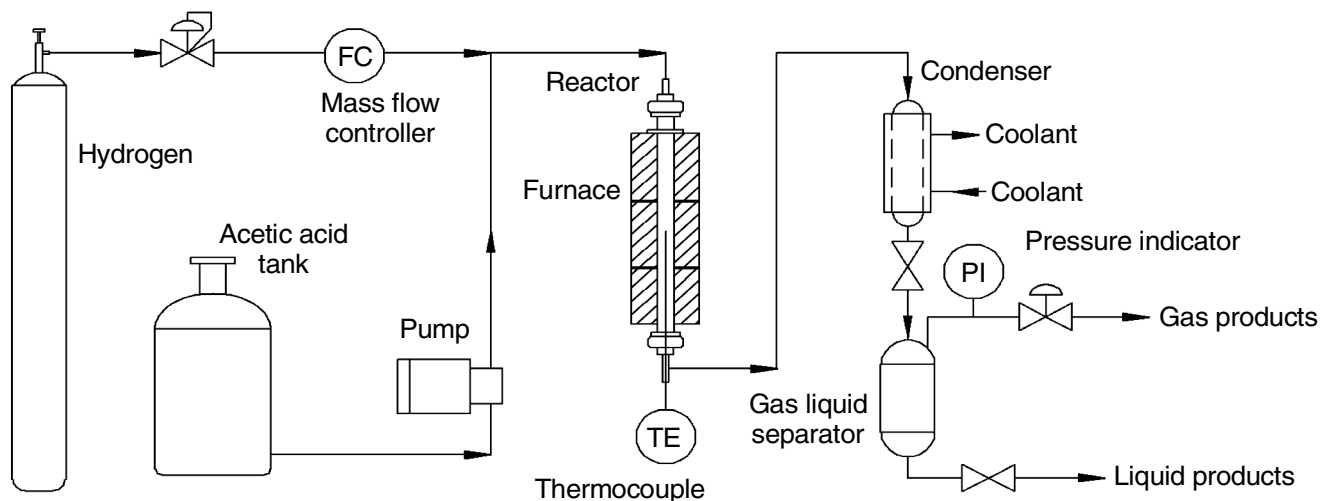


Fig. 1. Schematic diagram of acetic acid hydrogenation system

the bottom of tank, while the gas products were discharged into the vent system from the top of tank.

Analysis: During the experiments, the liquid products were taken out every 4 h for analysis by off-line Agilent Technologies model 7890A GC-FID with an Innowax19091N-133 column (30 m length \times 0.25 mm inner diameter \times 0.25 μ m film thickness). The column temperature was ramped from an initial oven temperature of 40 to 80 $^{\circ}$ C with a heating rate of 2 $^{\circ}$ C min^{-1} , then heated to 125 $^{\circ}$ C at 6 $^{\circ}$ C min^{-1} . Hydrogen served as the carrier gas at a flow rate of 30 mL min^{-1} .

Pre-experiments: The study of intrinsic kinetics needs to eliminate the influences of internal and external diffusion first. To investigate the effects of internal diffusion of reaction, we loaded reactor with the same amount of catalyst with particle size (dp) of 4.1, 1.3 and 0.6 mm. The acetic acid conversions (x) were obtained and correlated with the particle sizes of catalyst. All the experiments were carried out at conditions as follow: reaction temperature (t) of 275 $^{\circ}$ C, pressure (p) of 2.5 MPa, the space velocity (sv) of acetic acid (the ratio of volumetric flow rate of acetic acid to volume of catalyst loaded, space velocity) of 0.6 h^{-1} , the mole ratio of hydrogen to acetic acid (H/AC) of 16. The results as plotted in Fig. 2 show that the conversion of acetic acid is increased with the decrease of catalyst particle size, indicating the effects of the internal diffusion are reduced. The deviation of acetic acid reaction conversions on the catalyst with particle size of 1.3 mm and 0.6 mm is less than 1 %, which denotes the effect of internal diffusion has been basically eliminated. In the kinetics experiments, the catalyst was ground to particle size of 0.6 mm.

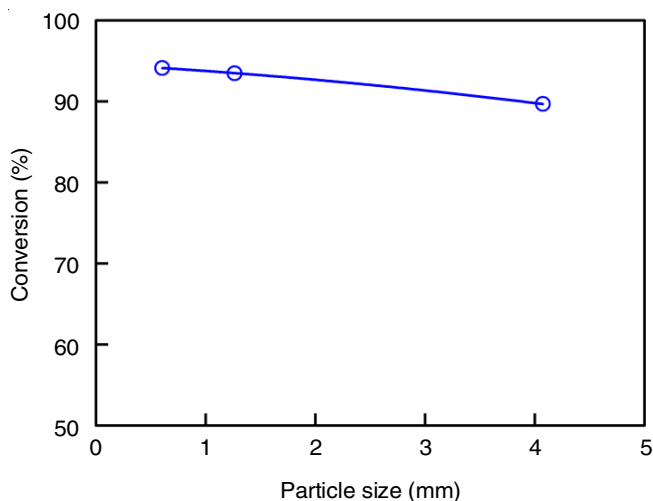


Fig. 2. Conversion in various particle sizes

To eliminate the effect of external diffusion, we conducted reactions in two fixed bed reactors (reactor A and B) with the same size and configuration to ensure comparability. The amount of catalyst used in reactor B was 60 % of the catalyst amount used in reactor A. Two sets of data were obtained under the following conditions: $t = 325$ $^{\circ}$ C, $p = 2.5$ MPa, space velocity = 0.3 ~ 0.9 h^{-1} , H/AC = 16, and the ratio of total feeding mole flow to the mass of catalyst (F/w) was the same between reactor A and B, so that the linear velocity of the feed in reactor B was slower than that in A. The acetic acid conversion data collected with various F/w ratios in both reactor A and B are

shown in Fig. 3. The results show that as increased F/w, the deviation of conversion obtained from reactor A and B was gradually reduced till the conversions obtained in two reactors became almost identical when the F/w was higher than 0.45 $\text{mol g}^{-1} \text{h}^{-1}$. The deviation was decreased to less 1 % at F/w of 0.33 $\text{mol g}^{-1} \text{h}^{-1}$, corresponding to the linear velocity of 0.19 cm s^{-1} in reactor B. Therefore, in this kinetics study, the total feeding mole flow was determined as faster than 0.33 $\text{mol g}^{-1} \text{h}^{-1}$ (or the linear velocity was faster than 0.19 cm s^{-1}).

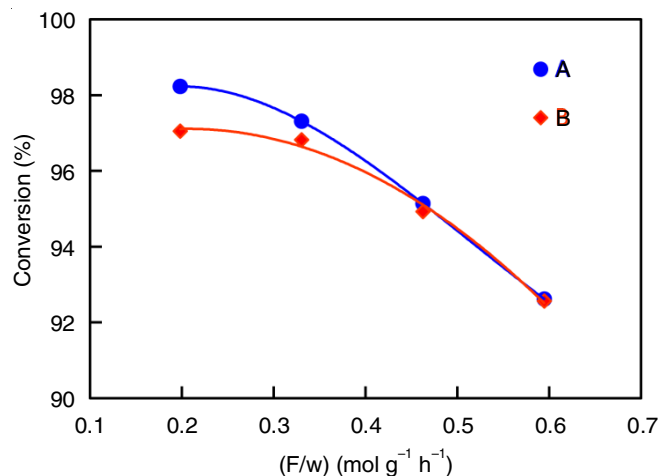


Fig. 3. Conversion in various F/w of reactor A and B

Design of experiments: The kinetics experiments were carried out in a fixed bed reactor system as shown in Fig. 1. The tests were performed at various combinations of the conditions as shown in Table-1. Totally 45 sets of data were collected for the kinetics study. According to the conditions at 0.344 MPa (a) the maximum partial pressure, the boiling point temperature of acetic acid is 196.7 $^{\circ}$ C [30] which is lower than the minimum reaction temperature 250 $^{\circ}$ C, implying the reaction was studied in the vapour phase.

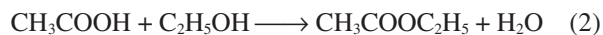
TABLE-1 RANGE OF PROCESS CONDITIONS				
Level number	Process conditions			
	t ($^{\circ}$ C)	p (MPa)	sv (h^{-1})	H/AC 1
L1	250	1.5	0.3	8
L2	275	2.0	0.6	12
L3	300	2.5	0.9	16
L4	325	3.0	1.2	20

sv = space velocity

RESULTS AND DISCUSSION

Total experimental error of acetic acid conversion is about 0.38 %, while the total experimental error of ethanol selectivity is 0.24 %. When the reaction temperature was lower than 300 $^{\circ}$ C, the total selectivity of ethanol and ethyl acetate was higher than 97.5 %, the selectivity of acetaldehyde was lower than 2.5 %, and the total by-products was lower than 0.5 %. The selectivity of acetaldehyde significantly related to the reaction temperature, when the temperature was increased to 325 $^{\circ}$ C, acetaldehyde selectivity was raised up to 6 % while the total selectivity of ethanol and ethyl acetate was around 93 %. In

order to simplify the kinetic model, it was assumed that only products are ethanol and ethyl acetate. Therefore, over present catalyst, there are two dominant reactions investigated:



Effect of reaction conditions

Temperature: The effect of reaction temperature on the activity and selectivity was studied at 275, 300 and 325 °C (Fig. 4). The results show that the conversion increases slowly with increasing the reaction temperature, while the selectivity of ethanol drops dramatically. The trend of selectivity with the reaction temperature is against that of conversion, which is similar with the published results [26,31]. It indicates that rising temperature leads to the promotion of the reaction rates of hydrogenation and esterification, but esterification rate is more sensitive to temperature than hydrogenation.

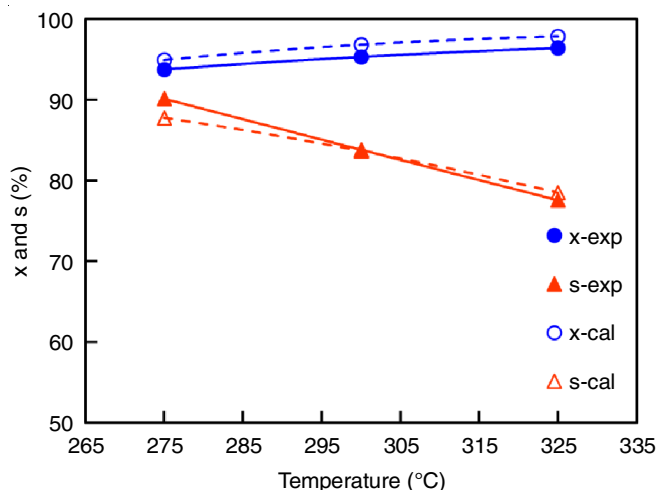


Fig. 4. Effect of temperature (condition: $p = 2.5$ MPa, $sv = 0.6$ h⁻¹, $H/AC = 16$)

Reaction pressure: The impact of reaction pressure was studied at 2.0, 2.5 and 3.0 MPa as displayed in Fig. 5. Both the conversion and the selectivity increased gradually with the increase of pressure. For gas phase reactions, partial pressures of reactants have a positive effect on reaction rate. The reduc-

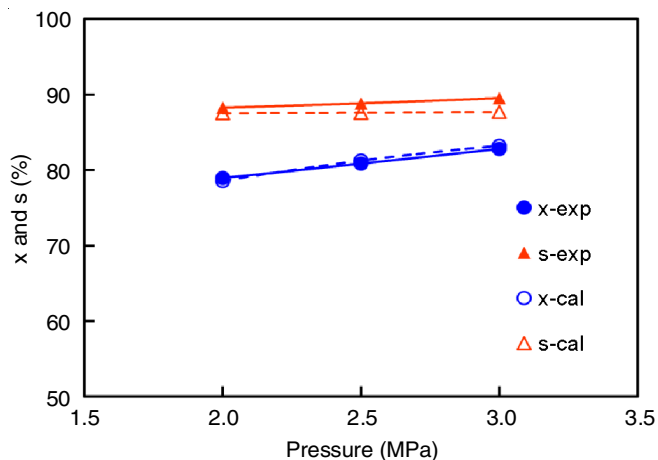


Fig. 5. Effect of pressure (condition: $t = 275$ °C, $sv = 1.2$ h⁻¹, $H/AC = 16$)

tion of acetic acid to ethanol and the esterification of acetic acid with ethanol to ethyl acetate are two chain reactions. The first one is a molecular number reduced reaction while the molecular number of the second reaction is constant. The increase of pressure allows the hydrogenation equilibrium to proceed to the right side of the equation, which is beneficial to the production of ethanol.

Acetic acid space velocity: The effect of space velocity of acetic acid was studied at 0.3, 0.6, 0.9 and 1.2 h⁻¹ as displayed in Fig. 6, the conversion dropped significantly with the rise of space velocity, while the selectivity of ethanol increased gradually. That is because the residence time reduced with the increase of space velocity which results in lower selectivity of ethyl acetate *via* secondary esterification reaction. The selectivity deviation of ethanol and ethyl acetate indicates that the acetic acid hydrogenation rate and esterification rate are different at different space velocity.

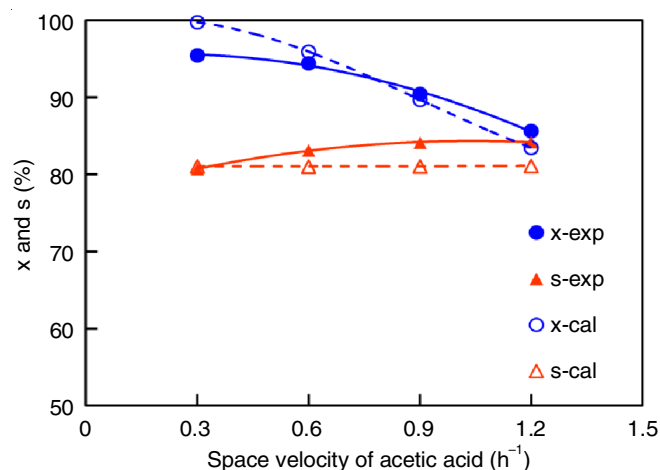


Fig. 6. Effect of acetic acid space velocity (Condition: $t = 300$ °C, $p = 2.0$ MPa, $H/AC = 12$)

Mole ratio of hydrogen to acetic acid: As shown in Fig. 7, acetic acid conversion decreased slightly but ethanol selectivity increased when the H/AC ratio was increased from 8 to 12, while the selectivity of ethanol increased slowly. When the total reaction pressure was the same and the H/AC ratio was increased, the partial pressure of hydrogen increased accom-

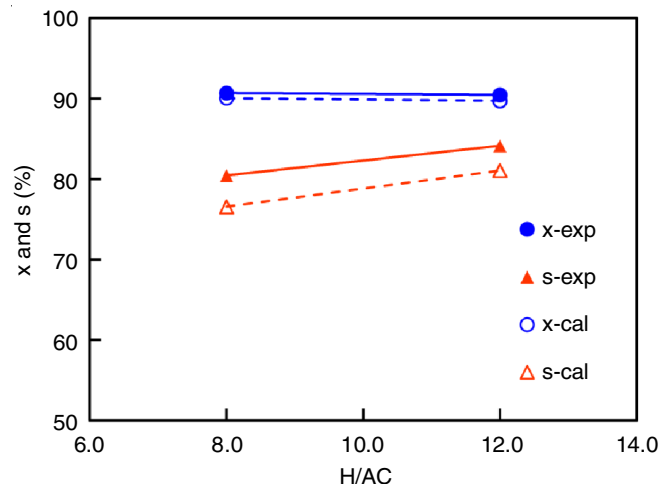
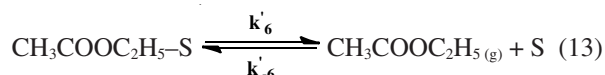
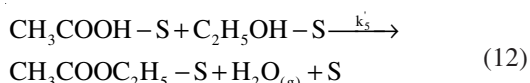
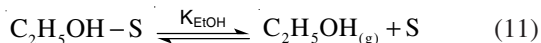
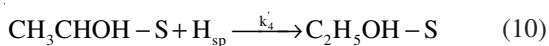
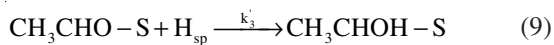
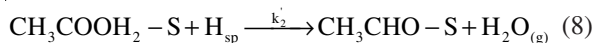
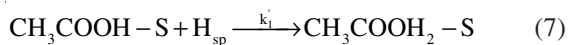
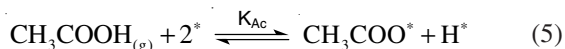


Fig. 7. Effect of mole ratio of hydrogen to acetic acid (Condition: $t = 300$ °C, $p = 2.0$ MPa, $sv = 0.9$ h⁻¹)

panied with the decrease of the partial pressure of acetic acid. Because hydrogen was always in excess in the reaction system, the effect of increasing hydrogen partial pressure was not able to overtake the negative effect of reducing acetic acid partial pressure. Moreover, the shorter residence time with the increase of H/AC ratio should also be taken into account.

Kinetics model and regression: Previous kinetic studies of acetic acid hydrogenation over bimetallic catalysts showed that the reaction can be described by a Langmuir-Hinshelwood-type mechanism involving two types of active sites, one is on the metal to activate hydrogen and another one is on the oxide to adsorb and activate acetic acid [19,27].

Based on the reported results, a Langmuir-Hinshelwood-type catalytic elementary reaction sequence was proposed as in the following eqns. 3-13:



where * and S represent catalytic sites on the metal and oxide surface, respectively k' is the rate coefficients of reaction, and K is the equilibrium adsorption constants.

The investigations showed that the addition of first H atom to an acetate species is the rate-determining steps of the sequence of elementary steps used to describe acetic acid reduction over Pt/TiO₂ [19,22]. The kinetics and mechanism investigations of acetic acid esterification with ethanol on four zeolites by Bedard and co-workers [32] showed that experiments data were consistent with the formation of an energetically favourable acetic acid and ethanol complex adsorbed on the zeolite active site and both are involved in the rate-determining step. Applying the steady-state approximation to the surface intermediates, and suggesting that both eqns. 7 and 12 are the rate-determining steps.

The activity of hydrogenation and esterification together determined the rate of acetic acid conversion, *i.e.*, the overall rate of formation of ethanol and ethyl acetate as shown in eqns. 14-16:

$$r_{\text{HOAc}} = r_1 + r_2 \quad (14)$$

$$r_1 = k'_1 \theta_{\text{HOAc}} C_{\text{H}} \quad (15)$$

$$r_2 = k'_5 \theta_{\text{HOAc}} \theta_{\text{EtOH}} \quad (16)$$

where θ_i is the fractional surface coverage of species i , θ_{HOAc} is the fractional surface coverage of acetic acid on the oxide surface, θ_{EtOH} is the fractional surface coverage of ethanol on the oxide surface, C_{H} is the concentration of hydrogen atoms on the sites of oxide surface.

The equilibrium expressions representing adsorption on the metal surface can be obtained from eqns. 3 and 5:

$$K_{\text{H}_2} = \frac{\theta_{\text{H}}^2}{P_{\text{H}_2} \theta_*^2} \quad (17)$$

$$K_{\text{Ac}} = \frac{\theta_{\text{Ac}} \theta_{\text{H}}}{P_{\text{HOAc}} \theta_*^2} \quad (18)$$

where P_i is the partial pressure of species i , subscripts H, Ac and * represent hydrogen atoms, acetate and vacant sites on the metal surface.

The equilibrium expressions representing adsorption on the oxide surface can be obtained from eqns. 6 and 11:

$$K_{\text{HOAc}} = \frac{\theta_{\text{HOAc}}}{P_{\text{HOAc}} \theta_{\text{S}}} \quad (19)$$

$$K_{\text{EtOH}} = \frac{\theta_{\text{EtOH}}}{P_{\text{EtOH}} \theta_{\text{S}}} \quad (20)$$

where subscripts HOAc, EtOH and S represent acetic acid, ethanol and vacant sites on the oxide surface.

It is assumed that adsorbed hydrogen atoms (H^*) and adsorbed acetate species (CH_3COO^*) are the predominant surface species on metal sites; while the molecular acetic acid and ethanol are the dominated surface intermediates on the oxide surface sites. Two balances of the fractional surface coverage on metal and oxide are given in eqns. 21 and 22:

$$\theta_{\text{H}} + \theta_{\text{Ac}} + \theta_* = 1 \quad (21)$$

$$\theta_{\text{HOAc}} + \theta_{\text{EtOH}} + \theta_{\text{S}} = 1 \quad (22)$$

The expression of θ_* is given in eqn. 23 evaluated from eqns. 17, 18 and 21:

$$\theta_* = \frac{1}{1 + \sqrt{K_{\text{H}_2} P_{\text{H}_2}} + \frac{K_{\text{Ac}} P_{\text{HOAc}}}{\sqrt{K_{\text{H}_2} P_{\text{H}_2}}}} \quad (23)$$

The expression of θ_{S} is given in eqn. 24 evaluated from eqns. 19, 20 and 22:

$$\theta_{\text{S}} = \frac{1}{1 + K_{\text{HOAc}} P_{\text{HOAc}} + K_{\text{EtOH}} P_{\text{EtOH}}} \quad (24)$$

The equilibrium expressions for H atom concentration on the oxide surface can be obtained from eqn. 4:

$$K_{sp} = \frac{C_{\text{H}}}{\theta_{\text{H}}} \quad (25)$$

The final rate expression of acetic acid disappearance is obtained by substituting eqns. 17-20 and eqns. 23-25 into eqns. 15 and 16 to give

$$r_1 = \frac{k'_1 K_{\text{HOAc}} K_{sp} \sqrt{K_{\text{H}_2} P_{\text{HOAc}}} \sqrt{P_{\text{H}_2}}}{(1 + K_{\text{HOAc}} P_{\text{HOAc}} + K_{\text{EtOH}} P_{\text{EtOH}}) \left(1 + \sqrt{K_{\text{H}_2} P_{\text{H}_2}} \frac{K_{\text{Ac}}}{\sqrt{K_{\text{H}_2} P_{\text{H}_2}}} \frac{P_{\text{HOAc}}}{\sqrt{P_{\text{H}_2}}} \right)} \quad (26)$$

$$r_2 = \frac{k'_5 K_{\text{HOAc}} K_{\text{EtOH}} P_{\text{HOAc}} P_{\text{EtOH}}}{(1 + K_{\text{HOAc}} P_{\text{HOAc}} + K_{\text{EtOH}} P_{\text{EtOH}})^2} \quad (27)$$

The k' and K found in eqns. 26 and 27 can be written as:

$$k' = k_0 \exp\left(\frac{-E_a}{RT}\right) \quad (28)$$

$$K = \exp\left(\frac{\Delta S}{R} - \frac{\Delta H}{RT}\right) \quad (29)$$

where E_a is the activation energy of the element reaction, ΔH is the adsorption enthalpy, ΔS is the adsorption entropy, R is the gas constant with the value of $8.314 \text{ J mol}^{-1} \text{ K}^{-1}$, T is the thermodynamic temperature with the unit of K .

Considering that the fixed bed reactor as an ideal isothermal plug-flow reactor, the rate expression of acetic acid around one differential catalyst mass element (dw) is:

$$r_1 + r_2 = -\frac{dN_{\text{HOAc}}}{dw} = -\frac{d[N_{\text{HOAc}}^0(1-x)]}{dw} = N_{\text{HOAc}}^0 \frac{dx}{dw} \quad (30)$$

$$r_2 = \frac{dN_{\text{EtOAc}}}{dw} = \frac{d[N_{\text{HOAc}}^0 x(1-s)]}{2dw} = \frac{N_{\text{HOAc}}^0}{2} \left[\frac{(1-s)dx - xds}{dw} \right] \quad (31)$$

which can be integrated over the entire catalyst mass to give

$$x = \int_0^w \frac{r_1 + r_2}{N_{\text{HOAc}}^0} dw \quad (32)$$

$$s = \int_0^w \frac{(1-s)r_1 - (1+s)r_2}{xN_{\text{HOAc}}^0} dw \quad (33)$$

where N_{HOAc}^0 is the molar flow rate of acetic acid at the inlet of reactor.

Using a numerical integration method based on an explicit Runge-Kutta formula (function "ode45") and a least-square non-linear regression method (function "lsqcurvefit") which are built-in MATLAB, we obtained every k' and K founded in eqns. 26 and 27. These optimum parameters are given as follow:

$$k_1' = 2.985 \times 10^4 \exp\left(-\frac{47839}{RT}\right) \quad (34)$$

$$k_5' = 4.365 \times 10^3 \exp\left(-\frac{52411}{RT}\right) \quad (35)$$

$$K_{\text{HOAc}} = \exp\left(-8.452 - \frac{-27432}{RT}\right) \quad (36)$$

$$K_{\text{sp}} = \exp\left(-7.757 - \frac{-43879}{RT}\right) \quad (37)$$

$$K_{\text{H}_2} = \exp\left(-10.158 - \frac{-25865}{RT}\right) \quad (38)$$

$$K_{\text{EtOH}} = \exp\left(-5.427 - \frac{-44095}{RT}\right) \quad (39)$$

$$K_{\text{Ac}} = \exp\left(-15.401 - \frac{-71283}{RT}\right) \quad (40)$$

Model evaluation: The x and s given by eqns. 32 and 33 were fitted to the experimental data. A histogram bar chart of the residuals and a normal probability plot were created using MATLAB function "histfit" and "normplot". They are shown in Fig. 8a-b. The data appears along the reference line indicates that the residual data have a normal distribution. The comparison of the experimental and calculated x and s are showed in Figs. 9 and 10, and the distribution of relative error of x and s are also described in Figs. 11 and 12. The results show that the calculated values are in good fitting trend with the experimental values (blue and red scatters), and all the relative errors except one are less than 6%. In addition, both the coefficients and the adjusted coefficients of determination are calculated: for x , $R^2 = 0.9256$, $\bar{R}^2 = 0.8944$; for s , $R^2 = 0.9059$, $\bar{R}^2 = 0.8665$. The rate expression derived from this model gives the root-mean-square error (RMSE) of its predicted x and s to be 2.17 and 2.13%. It suggested that the proposed model fits the experimental data with an excellent goodness-of-fit.

The model should be mathematically reasonable and thermodynamically limited. The activation energy E_a of the element reaction must be positive, and the adsorption enthalpy ΔH should be negative. Both absolute values of $|E_a|$ and $|\Delta H|$ should be in the range of 24 to 240 kJ mol^{-1} . Some criteria comprised of three strong rules and two guidelines to evaluate whether rate parameters, such as the adsorption equilibrium

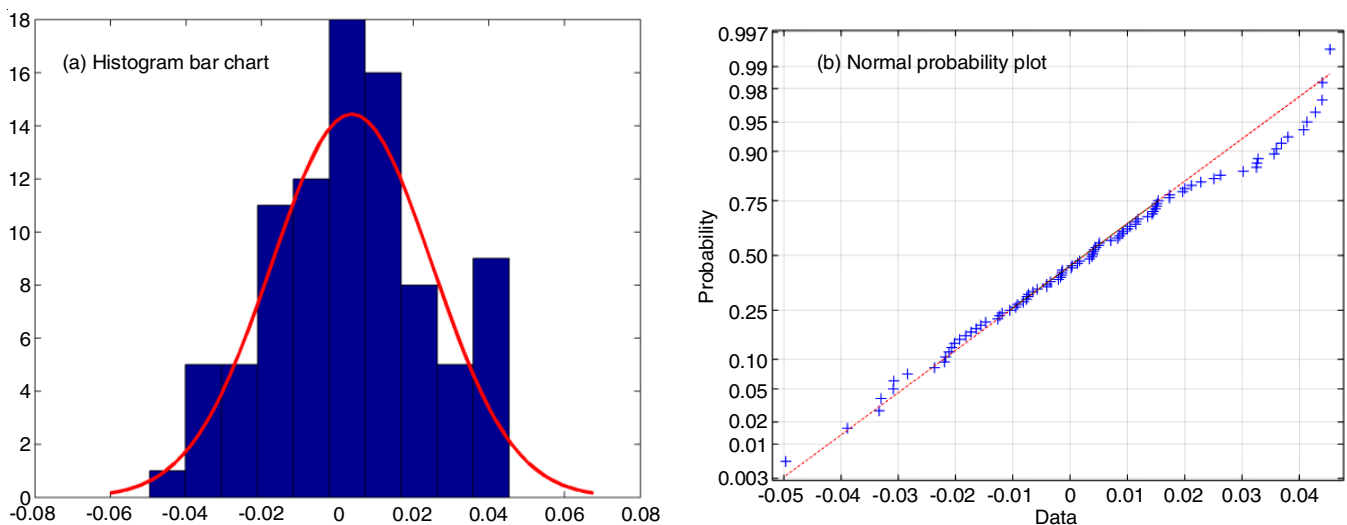


Fig. 8. Normality test of residuals

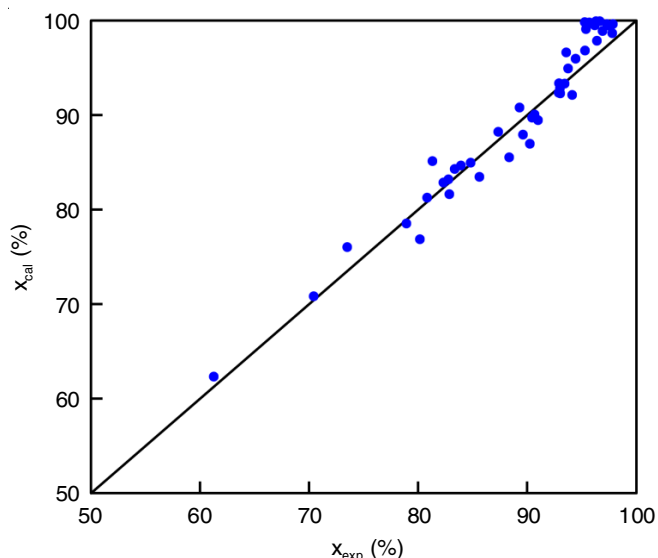


Fig. 9. Comparison between calculated and experimental conversion

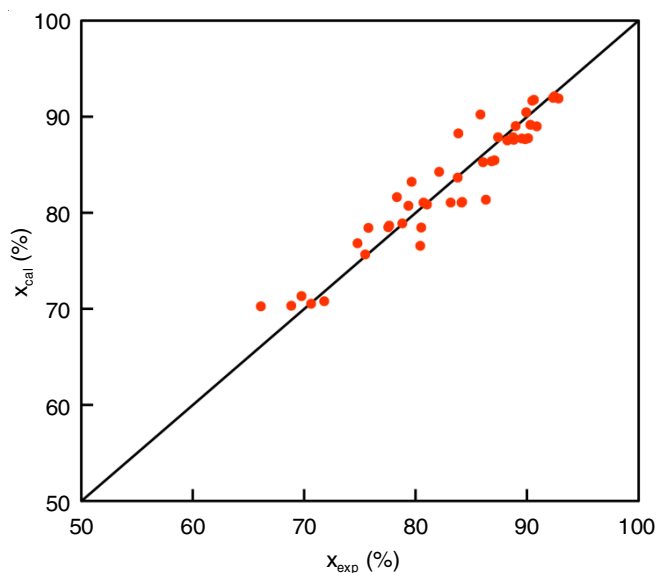


Fig. 10. Comparison between calculated and experimental selectivity

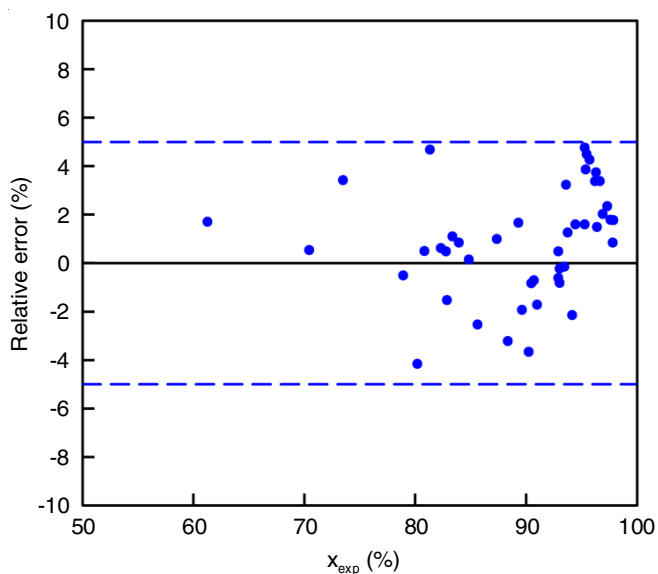


Fig. 11. Distribution of relative error of conversion

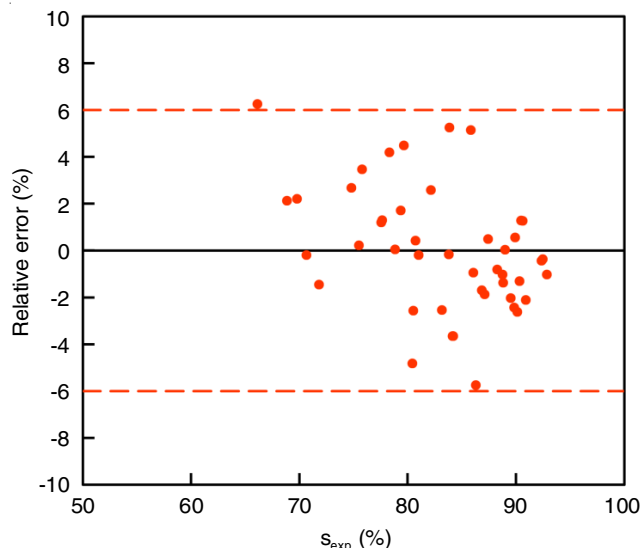


Fig. 12. Distribution of relative error of selectivity

constants appearing in the denominator of Langmuir isotherm involving the enthalpy and entropy of adsorption were proposed [33,34]. These criteria are listed in Table-2, where S_g is the standard total entropy in the gas phase. The calculated parameters are shown in Table-3.

TABLE-2
CRITERIA TO EVALUATE PARAMETERS

No.	Criteria unit (J mol^{-1})
C1	$24 \times 10^3 \leq E_a$ and $-\Delta H \leq 240 \times 10^3$
C2	$0 < -\Delta S < S_g$
C3	$41.8 \leq \Delta S \leq 51.0 - 0.0014\Delta H$

These results give the evidences of that model is suitable thermodynamically, also imply that dissociative acetic acid adsorption on the oxide surface is much weaker than that on metallic iron in accordance with previous report [22]. Future works such as the causes of a low selectivity of acetaldehyde, which is the intermediate of acetic acid to ethanol, and the mechanism of esterification over the multi-metallic catalysts still require more researches.

The profile of conversion of acetic acid, and the selectivity of ethanol and ethyl acetate along the axial direction of fixed bed reactor were calculated using present model. The result is shown in Fig. 13. The x-axis is the total mass fraction of catalyst along the flow direction. This pre-calculation can provide guidance for reactor design.

Conclusion

The hydrogenation of acetic acid to ethanol was conducted in a fixed bed reactor. The pre-experiments results show that the influence of internal diffusion and external diffusion could be mostly eliminated by using a catalyst with the particle size less than 1.3 mm and keeping the linear velocity of greater than 0.19 cm s^{-1} . The kinetics experiments were investigated at 275-325 °C, 1.5-3.0 MPa, 0.3-1.2 h^{-1} of acetic acid space velocity (sv) and 8-20 of mole ratio of hydrogen to acetic acid (H/AC). The results showed that increasing pressure and temperature, and reducing space velocity and H/AC can improve the conversion. On the other hand, reducing pressure and

TABLE-3
VALIDATION OF MODEL PARAMETERS

k or K	E_a or ΔH (kJ mol ⁻¹)	ΔS (J mol ⁻¹)	S_g (J mol ⁻¹)	$51.0 - 0.0014 \Delta H$ (J mol ⁻¹)
Hydrogenation rate parameter (k_1)	47.839	–	–	–
Esterification rate parameter (k_5)	52.411	–	–	–
Acetic acid on oxide (K_{HOAc})	-27.432	-70.3	293.4	86.4
H atoms migration to oxide (K_{sp})	-43.879	-64.5	114.7	98.0
Hydrogen on metal (K_{H_2})	-25.865	-84.5	130.7	89.5
Ethanol on oxide (K_{EtOH})	-44.095	-45.1	282.7	85.8
Acetic acid on metal (K_{AC})	-71.283	-128.0	293.4	145.3

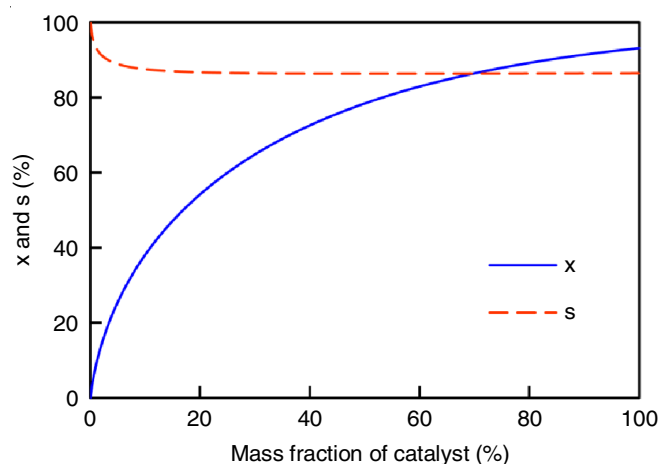


Fig. 13. Profile of x and s along the axial direction (Condition: $t = 285$ °C, $p = 3.0$ MPa, $sv = 0.8$ h⁻¹, $H/AC = 16$)

increasing temperature, liquid hourly space velocity (sv) and molar ratio of hydrogen to acetic acid (H/AC) can improve the selectivity of ethanol. The optimized model parameters were obtained by using a numerical integration method based on an explicit Runge-Kutta formula and a least-square non-linear optimization method. Calculated conversion and selectivity were in good agreement with experimental results. The parameters are consistent with three thermodynamic constraints. Studies in this paper provided evidence that the established intrinsic kinetic model was both mathematically and thermodynamically reasonable, and it could be used to guide reactor design.

ACKNOWLEDGEMENTS

This work was supported by National Key Research and Development Program of China (2018YFB0604703). The authors thank Ping Miao, Jihong Cheng, Yunjian Hu and Ruili Tong for discussions about of experimental methods.

CONFLICT OF INTEREST

The authors declare that there is no conflict of interests regarding the publication of this article.

REFERENCES

- X. Yan, O.R. Inderwildi, D.A. King and A.M. Boies, *Environ. Sci. Technol.*, **47**, 5535 (2013); <https://doi.org/10.1021/es305209a>.
- M. Gupta, M.L. Smith and J.J. Spivey, *ACS Catal.*, **1**, 641 (2011); <https://doi.org/10.1021/cs2001048>.
- E. Gnansounou and A. Dauriat, *J. Sci. Ind. Res. (India)*, **64**, 809 (2005).
- C.R. Nelson, M.A.D. Taylor, D.D. Davidson and L.M. Peters, *Olefin Hydration Process* (1951).
- H. Momose, K. Kusumoto, Y. Izumi and Y. Mizutani, *J. Catal.*, **77**, 23 (1982); [https://doi.org/10.1016/0021-9517\(82\)90142-7](https://doi.org/10.1016/0021-9517(82)90142-7).
- N. Katada, Y. Iseki, A. Shichi, N. Fujita, I. Ishino, K. Osaki, T. Torikai and M. Niwa, *Appl. Catal. A Gen.*, **349**, 55 (2008); <https://doi.org/10.1016/j.apcata.2008.07.005>.
- S. Kumar, N. Singh and R. Prasad, *Renew. Sustain. Energy Rev.*, **14**, 1830 (2010); <https://doi.org/10.1016/j.rser.2010.03.015>.
- G.W. Huber, S. Iborra and A. Corma, *Chem. Rev.*, **106**, 4044 (2006); <https://doi.org/10.1021/cr068360d>.
- Renewable Fuels Association, 2018 Ethanol Industry Outlook, 2018. <http://www.ethanolresponse.com/wp-content/uploads/2018/02/2018-RFA-Ethanol-Industry-Outlook.pdf>.
- Y. Zhang, X. San, N. Tsubaki, Y. Tan and J. Chen, *Ind. Eng. Chem. Res.*, **49**, 5485 (2010); <https://doi.org/10.1021/ie901882s>.
- X. Wu, Y. Wu, S. Zhang, H. Liu, L. Fu and J. Hao, *Environ. Pollut.*, **214**, 556 (2016); <https://doi.org/10.1016/j.envpol.2016.04.042>.
- Y. Wu, S. Zhang, J. Hao, H. Liu, X. Wu, J. Hu, T.J. Wallington, M.P. Walsh, K.M. Zhang and S. Stevanovic, *Sci. Total Environ.*, **574**, 332 (2017); <https://doi.org/10.1016/j.scitotenv.2016.09.040>.
- J. Jiao, J. Li and Y. Bai, *J. Clean. Prod.*, **180**, 832 (2018); <https://doi.org/10.1016/j.jclepro.2018.01.141>.
- H. Hao, Z. Liu, F. Zhao, J. Ren, S. Chang, K. Rong and J. Du, *Renew. Sustain. Energy Rev.*, **82**, 645 (2018); <https://doi.org/10.1016/j.rser.2017.09.045>.
- B. Qian, *Chem. Ind.*, **32**, 26 (2014); <https://doi.org/10.3969/j.issn.1673-9647.2014.02.006>.
- A.B. Stiles, F. Chen, J.B. Harrison, X. Hu, D.A. Storm and H.X. Yang, *Ind. Eng. Chem. Res.*, **30**, 811 (1991); <https://doi.org/10.1021/ie00053a002>.
- R.G. Herman, *Catal. Today*, **55**, 233 (2000); [https://doi.org/10.1016/S0920-5861\(99\)00246-1](https://doi.org/10.1016/S0920-5861(99)00246-1).
- N. Yoneda, S. Kusano, M. Yasui, P. Pujado and S. Wilcher, *Appl. Catal. A Gen.*, **221**, 253 (2001); [https://doi.org/10.1016/S0926-860X\(01\)00800-6](https://doi.org/10.1016/S0926-860X(01)00800-6).
- W. Rachmady and M. Vannice, *J. Catal.*, **192**, 322 (2000); <https://doi.org/10.1006/jcat.2000.2863>.
- W. Rachmady and M.A. Vannice, *J. Catal.*, **209**, 87 (2002); <https://doi.org/10.1006/jcat.2002.3623>.
- W. Rachmady and M.A. Vannice, *J. Catal.*, **207**, 317 (2002); <https://doi.org/10.1006/jcat.2002.3556>.
- W. Rachmady and M.A. Vannice, *J. Catal.*, **208**, 158 (2002); <https://doi.org/10.1006/jcat.2002.3560>.
- W. Rachmady and M.A. Vannice, *J. Catal.*, **208**, 170 (2002); <https://doi.org/10.1006/jcat.2002.3561>.
- V. Pallassana and M. Neurock, *J. Catal.*, **209**, 289 (2002); <https://doi.org/10.1006/jcat.2002.3585>.
- R. Alcalá, J.W. Shabaker, G.W. Huber, M.A. Sanchez-Castillo and J.A. Dumesic, *J. Phys. Chem. B*, **109**, 2074 (2005); <https://doi.org/10.1021/jp049354t>.
- K. Zhang, H. Zhang, H. Ma, W. Ying and D. Fang, *Catal. Lett.*, **144**, 691 (2014); <https://doi.org/10.1007/s10562-014-1210-z>.

27. K. Zhang, Ph.D. Thesis, Study on PtSn/Al₂O₃ Catalysts for Gas Phase Acetic Acid Hydrogenation to Ethanol, East China University of Science and Technology, Shanghai, China (2014).
28. G. Onyestyák, S. Harnos, A. Kaszonyi, M. Štolcová and D. Kalló, *Catal. Commun.*, **27**, 159 (2012); <https://doi.org/10.1016/j.catcom.2012.07.021>.
29. G. Onyestyák, S. Harnos, S. Klébert, M. Štolcová, A. Kaszonyi and D. Kalló, *Appl. Catal. A Gen.*, **464–465**, 313 (2013); <https://doi.org/10.1016/j.apcata.2013.05.042>.
30. R.D. Lide, CRC Handbook of Chemistry and Physics, CRC Press: Boca Raton, FL (2005).
31. S. Tian, J. Cheng, W. Di, Q. Chen, J. Long, X. Luo, Y. Hu, X. Meng, S. Sun and Q. Sun, *J. Fuel Chem. Technol.*, **44**, 862 (2016); <https://doi.org/10.3969/j.issn.0253-2409.2016.07.012>.
32. J. Bedard, H. Chiang and A. Bhan, *J. Catal.*, **290**, 210 (2012); <https://doi.org/10.1016/j.jcat.2012.03.020>.
33. M. Boudart, D.E. Mears and M.A. Vannice, *Ind. Chim. Belge.*, **32**, 281 (1967).
34. M.A. Vannice, S.H. Hyun, B. Kalpakci and W.C. Liauh, *J. Catal.*, **56**, 358 (1979); [https://doi.org/10.1016/0021-9517\(79\)90128-3](https://doi.org/10.1016/0021-9517(79)90128-3).